J. Phys. C: Solid State Phys., 17 (1984) 1643–1653. Printed in Great Britain

Phonon structure of amorphous germanium by inelastic electron tunnelling spectroscopy

M C Payne, A F J Levi†, W A Phillips, J C Inkson and C J Adkins
Cavendish Laboratory, Madingley Road, Cambridge CB3 0HE, UK

Received 22 September 1983, in final form 28 October 1983

Abstract. Measurements of inelastic electron tunnelling through barriers of amorphous germanium are reported. The data are analysed using a theory of the electron–phonon interaction which includes phonon correlations. The vibrational density of states obtained from the experimental data is in agreement with that expected for amorphous germanium containing a broad distribution of bond angle variations.

1. Introduction

Jaklevic and Lambe (1966) showed that tunnelling electrons could traverse an insulating barrier via inelastic collisions, giving up energy to vibrational modes in the barrier. These inelastic processes increased the tunnel current and appeared as peaks in d^2I/dV^2 versus bias voltage V. The peaks are related to the frequency distribution of barrier excitations. Since its discovery the technique has been used to study the vibrational modes of molecules chemisorbed onto oxide–metal interfaces. The interest in this inelastic electron tunnelling spectroscopy has centred on catalytic reactions, surface chemistry and trace substance detection (Wolfram 1978, Walmsley 1980, Weinberg 1982).

In this work these ideas are exploited in order to obtain information on the vibrational properties of the barrier as a whole. In previous papers work was reported on SiO_x (Levi *et al* 1983, Payne and Inkson 1983). This paper presents tunnelling measurements performed on junctions in which the barrier was amorphous germanium.

2. Experiment and results

The junctions used in this investigation were fabricated in an oil-pumped chamber with a liquid nitrogen trap. A 100 nm thick aluminium strip was deposited onto a clean glass substrate at room temperature. The barrier was formed by lightly oxidising the aluminium and subsequently evaporating germania from a resistively heated boat. The mean thickness of the barrier, as measured by a quartz microbalance crystal, was 3 nm. Films of this thickness are not continuous and so it was necessary to oxidise through the

† Now at Bell Laboratories, 600 Mountain Avenue, Murray Hill, NJ 07974, USA.

0022-3719/84/101643 + 11 $02.25

gaps. Oxidation was by glow discharge for a few minutes in 0.1 mm Hg of pure oxygen. To avoid edge effects from the electrodes and to define a distinct tunnelling region a masking arrangement allowed the deposition of a thicker layer of barrier material at the junction edges. Finally, a top electrode was evaporated to complete the device.

Electrical connections to the junctions were made using copper wires and indium pads. Accurate measurements of the d^2I/dV^2 characteristics were performed using standard bridge and modulation techniques (Adler and Straus 1975). This method of measuring the d^2I/dV^2 characteristics of the tunnel junctions was very sensitive. Typically, the d^2I/dV^2 characteristics could be measured to an accuracy of a few parts per thousand. The energy resolution of the tunnelling spectra was limited by the thermal smearing of the energies of the electrons in the electrodes (Klein *et al* 1973). Normally, measurements were carried out with the junctions at a temperature of 4.2 K, at which temperature the energy resolution was 2.0 meV. To confirm that the electron transport mechanism was indeed tunnelling, the temperature could be lowered below 1 K and the aluminium superconducting density of states observed in the junctions' I–V characteristics. A microcomputer-based system controlled data acquisition and also performed data manipulation tasks.

When the extent of oxidation in the fabrication stages was increased (increasing the amount of alumina), peaks associated with the vibrational modes of alumina were observed in the tunnelling spectrum. The data analysed in the following sections did not show any such peaks.

The spectra obtained from junctions where the top electrodes were lead, tin and zinc were similar, all showing broad features over a range of energy up to 120 meV, as expected for barriers of germania. In contrast, when aluminium was used to form the top electrode the spectrum was very different: there were no features above 50 meV and the d^2I/dV^2 characteristic was similar to that expected for pure amorphous germanium. It seems reasonable to assert that this behaviour is dependent on the reactivity of the metal used to complete the junction. The d^2I/dV^2 characteristic is evidence that when aluminium forms the top electrode the germania is reduced to produce a barrier of amorphous germanium. In this paper we only consider junctions in which the top electrode was aluminium. An example of this tunnelling data is given in figure 1(*a*). Figure 1(*b*) shows the tunnelling spectrum of figure 1(*a*) after subtraction of the smooth elastic tunnelling background (shown by the broken line in figure 1(*a*)) and averaging between positive and negative bias. There is negligible asymmetry in the peak heights between positive and negative bias and the data are reproducible between samples to better than 5%.

3. Theoretical

The vibrational density of states of the barrier material, $g(\omega)$, is related to the experimentally measured d^2I/dV^2 characteristic via the relation

$$(d^2I/dV^2)|_\omega \propto |M(\omega)|^2 g(\omega). \tag{1}$$

Determination of $g(\omega)$ from the experimental results requires knowledge of $M(\omega)$, the matrix element coupling tunnelling electrons to the phonons. As a first approximation, we may assume that the scattering from each atom adds incoherently. This assumption was used successfully for SiO_x (Payne and Inkson 1983) to relate the relative intensities of the optic vibrational modes where the displacements of nearest-neighbour atoms tend

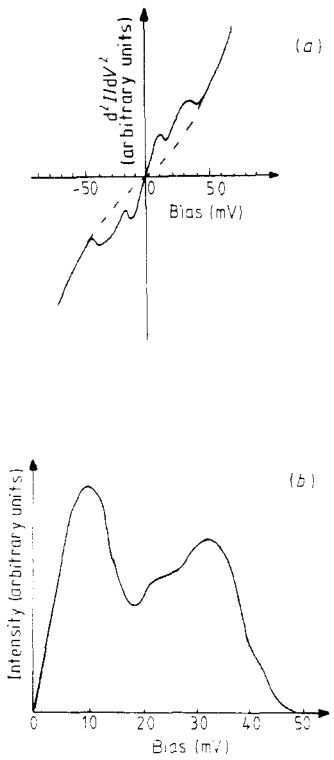

Figure 1. (*a*) The d^2I/dV^2 characteristic of the tunnel junction (full curve) showing the smooth elastic background (broken curve). (*b*) The d^2I/dV^2 characteristic after subtraction of the elastic background and averaging between positive and negative bias.

to be in opposite directions. The incoherent approximation therefore appears to give a good description of the relative scattering strengths of modes which have the same character. In the case of germanium, the main features of the vibrational spectrum arise from modes of different character, equivalent to the acoustic and optic modes of the crystal. Calculations for amorphous germanium (Alben *et al* 1975) suggest that the incoherent approximation cannot be used to compare the intensities of the optic modes to those of acoustic modes in which neighbouring atoms tend to vibrate in phase. This is confirmed by the inelastic spectrum obtained by multiplying d^2I/dV^2 by ω, the weighting factor for amorphous germanium calculated from the incoherent approximation. This spectrum gives too much weight to the optic modes. Correlations must be included in a calculation of $|M(\omega)|^2$.

The simplest method of including correlations is to adopt a bond model in which pairs of connected atoms are considered as the scattering unit. We refer to the combined scattering from the two atoms as bond scattering. The justification for the bond model is that it includes correlations resulting from the strongest inter-atomic force, the bond stretching force. The tetrahedral symmetry of bonds around every site, which is approximately maintained in the amorphous material (Etherington *et al* 1982), is an essential feature as it allows the atomic displacements to be projected onto a local coordinate system defined by the tetrahedral system of bonds. The disorder in amorphous germanium is primarily due to variations in the dihedral angles between adjacent

tetrahedral units. There is no quantitative description of the degree of disorder in the bond model for amorphous germanium beyond the assumption that the disorder is sufficient for the projected displacements of the atoms to be uncorrelated from bond to bond.

In central force models of $g(\omega)$ for crystalline germanium (Cochran 1965) and for amorphous germanium (Alben and Weaire 1972) the transverse modes correspond to δ function peaks in the vibrational density of states. The transverse acoustic (TA) modes occur at $\omega = 0$ and the transverse optic (TO) modes occur at $\omega = \omega_{max}$. In the bond model, the modes are described in terms of the projected displacements of neighbouring atoms along their common bond. TA modes correspond to atomic motions in which the bond length is constant so the projected displacements are equal in magnitude and in direction (figure 2(*a*)). Projected displacements in the TO modes are equal in magnitude but opposite in direction (figure 2(*b*)).

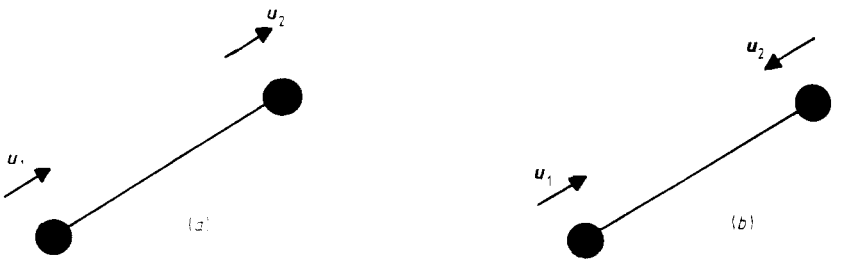

Figure 2. (*a*) The displacements of the atoms projected onto the common bond for the transverse acoustic modes in the central force model of amorphous germanium. (*b*) The projected displacements in the transverse optic modes.

Alben *et al* (1975) used this model to calculate the ratio of inelastic neutron scattering from the TA and TO modes at fixed scattering wavevector $\boldsymbol{Q}$. In the inelastic electron tunnelling experiment there is a range of scattering wavevectors so we must sum over these to obtain the total scattering. We proceed by first evaluating the contribution to the scattering from a single scattering vector $\boldsymbol{Q}$.

Suppose the tunnelling electron interacts with a phonon of frequency ω. The interaction results from the potential produced by the atomic displacements arising from the presence of the phonon. If an atom at the origin produces a potential $V(\boldsymbol{r})$, then, when it is displaced to a position given by $\boldsymbol{r}' = \boldsymbol{u}\exp(\mathrm{i}\omega t)$ the resulting potential $U(\boldsymbol{r}, t)$ is simply the potential produced by the atom centred at $\boldsymbol{r}'$ rather than the origin

$$U(\boldsymbol{r}, t) = V(\boldsymbol{r} - \boldsymbol{u}\exp(\mathrm{i}\omega t)). \tag{2}$$

If the potential is continuous and the displacement is small then $U(\boldsymbol{r}, t)$ is given by

$$U(\boldsymbol{r}, t) \approx V(\boldsymbol{r}) - \boldsymbol{u}\cdot\nabla V(\boldsymbol{r})\exp(\mathrm{i}\omega t). \tag{3}$$

Thus the electron sees a time-dependent potential from which it may inelastically scatter. If the Fourier transform of the time-dependent potential is taken we obtain the scattering potential in wavevector space

$$U(\boldsymbol{Q}, t) = \boldsymbol{u}\cdot\boldsymbol{Q}V(\boldsymbol{Q})\exp(\mathrm{i}\omega t) \tag{4}$$

where $V(\boldsymbol{Q})$ is the component of the pseudopotential for the atom at wavevector $\boldsymbol{Q}$.

This is the standard result of pseudopotential theory for electron–phonon coupling (see Harrison 1966). The values of $V(\boldsymbol{Q})$ used in this calculation were taken from the tables given by Harrison.

Now that a model for the transverse phonons and an expression for the electron–phonon coupling has been established, the matrix elements for the TA and TO modes may be calculated. The method projects the atomic displacements onto the tetrahedral bonds using the unit dyadic

$$\mathbf{I} = \tfrac{3}{4}\sum_{\Delta} \boldsymbol{e}_{\Delta}\boldsymbol{e}_{\Delta} \tag{5}$$

where Δ is a bond index for the atom, $\boldsymbol{e}_{\Delta}$ are unit vectors along the bonds and the sum is over the four tetrahedral bonds at any particular atom. Once the atomic motions have been projected onto the bonds, the bond scattering is calculated by summing the contributions to the scattering from the two atoms joined by the bond, including the phase factors $\exp(\mathrm{i}\boldsymbol{Q}\cdot\boldsymbol{r})$ (figure 3). Within the model atomic motions are correlated only

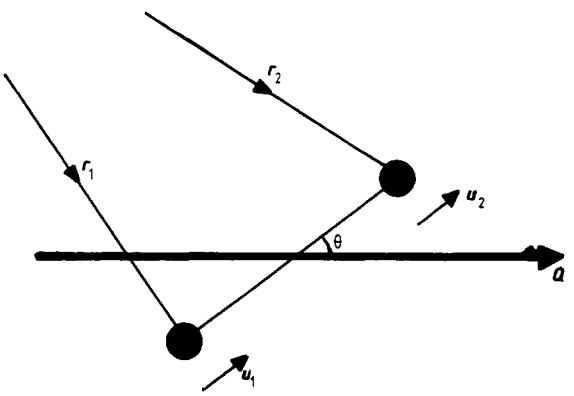

Figure 3. The scattering from a bond at wavevector $\boldsymbol{Q}$. $\boldsymbol{r}_1$ and $\boldsymbol{r}_2$ are the position vectors of the atoms, l is the bond length and θ is the angle between $\boldsymbol{Q}$ and the bond. The scattering from bond to bond is assumed to be incoherent.

along a single bond. The phase factor must be included to calculate the bond scattering but the total scattering is obtained by an incoherent addition of the bond scatterings. The matrix element for the bond scattering is

$$m(\boldsymbol{Q})_b = \tfrac{3}{4}(\boldsymbol{u}_1\exp(\mathrm{i}\boldsymbol{Q}\cdot\boldsymbol{r}_1) + \boldsymbol{u}_2\exp(\mathrm{i}\boldsymbol{Q}\cdot\boldsymbol{r}_2))\cdot\boldsymbol{Q}V(\boldsymbol{Q}) \tag{6}$$

where b is a bond label, $\boldsymbol{u}_1$ and $\boldsymbol{u}_2$ are the projected displacements and $\boldsymbol{r}_1$ and $\boldsymbol{r}_2$ are the position vectors of the two atoms. From the model, $\boldsymbol{u}_1 = \boldsymbol{u}_2$ for the TA modes, and $\boldsymbol{u}_1 = -\boldsymbol{u}_2$ for the TO modes. Hence the matrix element squared for the TA modes is

$$|m(\boldsymbol{Q}, \omega_{\mathrm{TA}})_b|^2 = \tfrac{9}{4}(u^b_{\mathrm{TA}})^2|V(\boldsymbol{Q})|^2Q^2\cos^2\theta\cos^2\left[\frac{Ql\cos\theta}{2}\right] \tag{7}$$

and for the TO modes it is

$$|m(\boldsymbol{Q}, \omega_{\mathrm{TO}})_b|^2 = \tfrac{9}{4}(u^b_{\mathrm{TO}})^2|V(\boldsymbol{Q})|^2Q^2\cos^2\theta\sin^2\left[\frac{Ql\cos\theta}{2}\right] \tag{8}$$

where θ is the angle between $\boldsymbol{Q}$ and the bond and l is the bond length. u^b_{TA} and u^b_{TO} are the amplitudes of the projected displacements for bond b in the TA and TO modes respectively. The scattering from each bond adds incoherently

$$|M(\boldsymbol{Q}, \omega)|^2 = \sum_b |m(\boldsymbol{Q}, \omega)_b|^2. \tag{9}$$

This sum is equivalent to averaging $|m(\boldsymbol{Q}, \omega)_b|^2$ over all orientations of bonds and summing over all values of the square of the amplitude of the projected displacements which gives the average square amplitude, $\overline{u^2}$, multiplied by the number of bonds N. Hence equation (9) may be rewritten

$$|M(\boldsymbol{Q}, \omega)|^2 = \sum_{(u_b)^2} \int_0^{\varphi=2\pi} \int_0^{\theta=\pi} |m(\boldsymbol{Q}, \omega)_b|^2 \frac{\sin\theta \,\mathrm{d}\theta \,\mathrm{d}\varphi}{4\pi}. \tag{10}$$

The intensity of scattering at given $\boldsymbol{Q}$ and ω is obtained by summing the contributions due to scatterings from every occupied state at energy ε, based on one side of the barrier, to every unoccupied state at energy $\varepsilon - \hbar\omega$, based on the other side of the barrier, resulting from the overlap of the evanescent tails of their wavefunctions in the barrier. The dependence of this function on ω and the voltage applied to the junction, V, produces the peaks in $\mathrm{d}^2I/\mathrm{d}V^2$. Payne and Inkson (1983) showed that the $\boldsymbol{Q}$-dependent part of this function, $f(\boldsymbol{Q})$, is almost independent of ω and V. The phonon energies are small compared with the energy range of the bandstructure, so all the initial and final states involved in the inelastic tunnelling have energies close to the Fermi levels in the electrodes and the evanescent wavefunctions can be assumed not to vary over the range of ω and V. Hence, $f(\boldsymbol{Q})$ can be calculated from the overlap at wavevector $\boldsymbol{Q}$ of the evanescent wavefunctions ψ_{i} and ψ_{f} connected to electronic states at the Fermi levels in the initial and final electrode respectively, summed over all the states at the Fermi levels

$$f(\boldsymbol{Q}) = \sum_{\mathrm{i,f}} \left| \int_{\mathrm{Barrier}} \psi_{\mathrm{f}}^*(\boldsymbol{r}) \exp(\mathrm{i}\boldsymbol{Q}\cdot\boldsymbol{r}) \, \psi_{\mathrm{i}}(\boldsymbol{r}) \, \mathrm{d}^3\boldsymbol{r} \right|^2. \tag{11}$$

However we still need to know ψ_{i} and ψ_{f} to calculate $f(\boldsymbol{Q})$ exactly. To deduce the form of these tunnelling wavefunctions we start by considering the bandstructure of crystalline germanium. This bandstructure is most easily understood in the Jones zone construction (Heine and Jones 1969). The Jones zone has twelve similar zone faces and encloses four electronic states per atom. As Heine and Jones point out, its shape does not differ greatly from that of a sphere. The Fermi surface of crystalline germanium corresponds to the surface of the Jones zone so there is an energy gap at every point on the Jones zone surface. The important states for tunnelling will be those with small effective mass in the tunnelling direction and will be those where this direction is normal to the zone (Burt and Inkson 1976, Inkson 1980). These states are, predominantly, combinations of plane waves whose wavevectors lie on the surface of the zone. Hence, the dominant tunnelling states are those composed of plane waves on the surface of the Jones zone. The model we adopt for amorphous germanium uses a spherical zone with radius k_{F}, the Fermi wavenumber of a free electron gas with density equal to the electronic density in amorphous germanium. As in the crystalline case, there is a gap at every point on the surface of the zone and the states on either side of the gap provide basis states for the evanescent solutions at the tunnelling energy in the gap. These basis states are not simple combinations of a few plane waves because the potential due to the ion cores is not restricted to reciprocal

lattice wavevectors and will couple a range of plane wave states. However, the plane waves contributing to any particular state must have energies that do not differ greatly from the energy of the state. Therefore, the plane wave components in each basis state will come from a spherical shell in wavevector space corresponding to nearly degenerate plane wave states. At the gap energy, the thickness of the shell, Δk, is calculated by assuming that all the plane wave states which are effectively degenerate, as a result of the potential produced by the ion cores, contribute to the basis states. This potential is given by the value of the bandgap which has been measured by Spicer (1974) as 1.5 eV. This is related to Δk by

$$\hbar^2/2m[(k_F + \tfrac{1}{2}\Delta k)^2 - (k_F - \tfrac{1}{2}\Delta k)^2] = 1.5 \text{ eV}. \tag{12}$$

The value of k_F is calculated from the value of the free electron Fermi energy, ε_F, which we approximate by the value of valence bandwidth. This is equal to 12 eV (Spicer 1974), so

$$\varepsilon_F = \frac{\hbar^2 k_F^2}{2m} \approx 12 \text{ eV}. \tag{13}$$

Combining equations (12) and (13) gives

$$\Delta k \approx \tfrac{1}{16} k_F. \tag{14}$$

Hence, the evanescent wavefunctions in the gap will be composed of plane waves with wavevectors lying within this shell. The sum over all the important tunnelling states with small evanescent decay rates produces a uniform density of plane wave components in the shell. In this model the value of $f(\boldsymbol{Q})$ is equal to the volume of intersection of two spherical shells of radius k_F and thickness Δk with their centres separated by $\boldsymbol{Q}$. The two shells correspond to the plane wave components from all the initial states, ψ_i, and final states, ψ_f, which have small evanescent decay rates. There is an upper limit to $f(\boldsymbol{Q})$ at $Q = 2k_F + \Delta k$, as beyond this value of Q the shells no longer intersect. From this model $f(\boldsymbol{Q})$ is given by

$$\begin{aligned} f(\boldsymbol{Q}) &= B4\pi k_F^2 \Delta k && Q \ll \Delta k \\ &= B\pi k_F^2 \Delta k^2/Q && \Delta k < Q < 2k_F - \Delta k \\ &= 0 && Q > 2k_F + \Delta k \end{aligned} \tag{15}$$

where B is a constant. In the range not covered by equation (15), between $2k_F - \Delta k$ and $2k_F + \Delta k$ there is a small increase in $f(Q)$.

The total scattering is obtained by integrating the square of the $\boldsymbol{Q}$-dependent matrix element over the distribution of scattering vectors given by equation (15).

$$|M(\omega)|^2 = \int |M(\boldsymbol{Q}, \omega)|^2 f(\boldsymbol{Q}) \, \mathrm{d}^3\boldsymbol{Q}. \tag{16}$$

The small Q contribution to this integral is negligible so the value of Δk is irrelevant providing $\Delta k \ll 2k_F$. Evaluating the integrals gives

$$|M(\omega_{TA})|^2 = C \times N\overline{u_{TA}^2} \tag{17}$$

and

$$|M(\omega_{TO})|^2 = C \times 2.1 \times N\overline{u_{TO}^2} \tag{18}$$

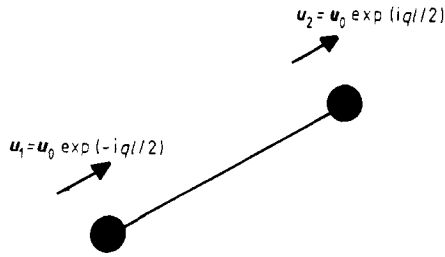

Figure 4. The bond model description of the longitudinal modes in the central force model. The projected displacements are related by a phase factor ql which determines the mode frequency.

where C is a constant.

The longitudinal modes correspond to a continuous band of frequencies. They can be treated in the bond model by introducing a phase factor ql between the projected displacements of the atoms joined by the bond (figure 4). The phonon frequency is related to this phase factor by equating the potential and kinetic energies:

$$\tfrac{1}{2}K|\exp(iql/2) - \exp(-iql/2)|^2(u^b_{\omega_L})^2 = \tfrac{3}{4}M\omega_L^2(u^b_{\omega_L})^2 \tag{19}$$

where M is the atomic mass and K is the bond force constant. This gives

$$\sin^2\left(\frac{ql}{2}\right) = \frac{8M}{3K}\omega_L^2 = \left(\frac{\omega_L}{\omega_{\max}}\right)^2. \tag{20}$$

Repeating the analysis and using equation (20) to replace ql by ω_L gives

$$|M(\omega_L)|^2 = C \times N\overline{u^2_{\omega_L}}\left[1.0 + 1.1\left(\frac{\omega_L}{\omega_{\max}}\right)^2\right]. \tag{21}$$

These results are valid for a central force model of the vibrational modes in amorphous germanium. Inclusion of the bond bending forces leaves the basic nature of the vibrational modes unchanged but broadens the δ-function peaks of the transverse modes into narrow bands. The matrix elements may be combined into a single frequency-dependent matrix element which applies to all the vibrational modes.

$$|M(\omega)|^2 = C \times N\overline{u^2_{\omega}}\left[1.0 + 1.1\left(\frac{\omega}{\omega_{\max}}\right)^2\right]. \tag{22}$$

Finally, $N\overline{u^2_{\omega}}$ is evaluated by equating the kinetic energy to the phonon energy:

$$\tfrac{3}{4}NM\overline{u^2_{\omega}}\omega^2 = \hbar\omega \tag{23}$$

$$N\overline{u^2_{\omega}} \propto 1/\omega \tag{24}$$

which gives

$$|M(\omega)|^2 \propto (1/\omega)[1.0 + 1.1(\omega/\omega_{\max})^2]. \tag{25}$$

Substituting equation (25) into equation (1) gives the vibrational density of states

$$g(\omega) \propto \left.\frac{d^2I}{dV^2}\right|_{\omega} \times \frac{\omega}{1.0 + 1.1(\omega/\omega_{\max})^2}. \tag{26}$$

The matrix element has been calculated assuming no correlation of the scattering from bond to bond. In the very low-frequency acoustic modes the amorphous material behaves as an elastic continuum and the phonons are plane-wave-like:

$$\boldsymbol{u}(\boldsymbol{r}) = \boldsymbol{u}_0 \exp \mathrm{i}[\boldsymbol{q} \cdot \boldsymbol{r} - \omega t]. \tag{27}$$

In this limit the disorder is no longer of any consequence and the assumption of no correlations is not valid. The momentum selection rule $\boldsymbol{Q} = \boldsymbol{q}$ applies, so the matrix element is given by

$$|M(\omega)|^2 \propto (1/\omega)[Q^2|V(\boldsymbol{Q})|^2]\,\delta(\boldsymbol{Q} - \boldsymbol{q}). \tag{28}$$

In the elastic continuum limit $q \propto \omega$ and $|V(\boldsymbol{Q})| \rightarrow$ constant as $\boldsymbol{Q} \rightarrow \boldsymbol{0}$. Therefore

$$|M(\omega)|^2 \propto \omega. \tag{29}$$

The value of the matrix element given by equation (29) will apply below a critical frequency. One must also expect some two-dimensional character to appear in the phonon density of states at low values of ω due to the finite width of the barrier. These effects will only become important below 5 meV. However, the weight in the vibrational density of states below 5 meV is very small, so we make a negligible error by using equation (25) only. In a finite width barrier, we expect contributions to $\mathrm{d}^2I/\mathrm{d}V^2$ from phonons associated with the electrode–barrier interfaces. It is not obvious how to include these phonons in the calculation of $|M(\omega)|^2$. However, there are no features in the experimental $\mathrm{d}^2I/\mathrm{d}V^2$ characteristics directly attributable to the interfaces. This is, perhaps, expected because the barrier and electrodes are reasonably matched acoustically. The contributions to $\mathrm{d}^2I/\mathrm{d}V^2$ from phonons associated with the interfaces appear to be small, so we feel justified in assuming that the tunnelling spectra are dominated by phonons which are characteristic of the amorphous germanium in the barriers.

4. The density of states

Multiplication of the data presented in figure 1(*b*) by $1/|M(\omega)|^2$ gives the vibrational density of states shown in figure 5(*a*). This is to be compared with the theoretically calculated $g(\omega)$ for a continuous random network model of amorphous germanium (Weaire and Taylor 1980) shown in figure 5(*b*). Raman and infrared spectra from thin films of amorphous germanium are reproduced in figures 5(*c*) and 5(*d*) respectively (Weaire and Taylor 1980). The Raman and infrared spectra have different (and unknown) energy dependences in their scattering matrix elements. Hence, these spectra do not give a quantitative measurement of $g(\omega)$.

The reduced tunnelling spectrum shown in figure 5(*a*) consists of a broad TA peak centred around 11 meV and a TO peak at 34 meV. There is also a broad shoulder extending from around 20 to 30 meV corresponding to longitudinal acoustic (LA) and longitudinal optic (LO) modes. These general features are similar to those appearing in the calculated spectrum shown in figure 5(*b*). However, the peaks in the calculated data are narrower than those in the inelastic electron tunnelling spectrum. It is also worth noting that unpublished inelastic neutron scattering data (Mook 1983) gives sharper peaks and more detailed structure in $g(\omega)$ than the tunnelling result. Meek (1977) calculated the vibrational density of states of amorphous germanium using the recursion method (Kelly 1980) and showed (i) that the TA and TO peaks were broadened

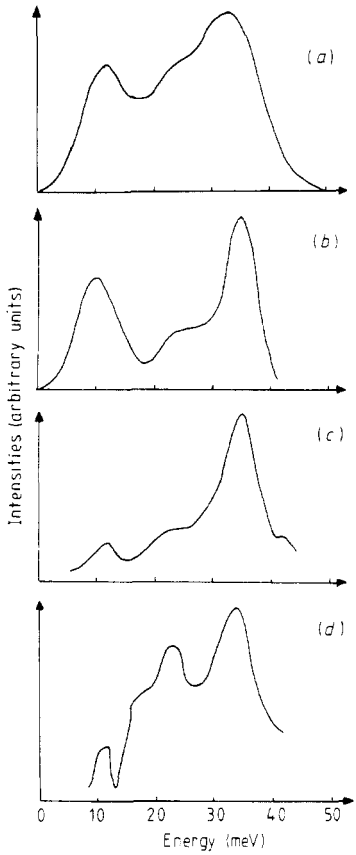

Figure 5. (*a*) The density of states, $g(\omega)$, for amorphous germanium (a-Ge) obtained by weighting the d^2I/dV^2 characteristic shown in figure 1(*b*). (*b*) $g(\omega)$ calculated for a network model of a-Ge. (*c*) Raman spectrum of a thin film of a-Ge. (*d*) Infrared spectrum of a thin film of a-Ge.

with the TO peak moving to a slightly higher frequency as the bond angle distortion increased, and (ii) that the dip in the density of states between the LA and LO modes, which is present when the bond angle variations are small, disappears. The spectrum in figure 5(*a*) shows broadened TA and TO peaks and no dip between the LA and LO modes. These are the characteristics of highly disordered amorphous germanium. This suggests that the very thin films of amorphous germanium that form the barriers in the tunnelling experiments contain a broader distribution of bond angle variations than the thicker films of amorphous germanium used in the optical and neutron experiments.

Finally, the inelastic tunnelling work of Ladan and Zylbersztejn (1972) using junctions of aluminium–germanium–tin should be mentioned. They obtained a noisy spectrum which had features similar to those expected for amorphous germanium. However, there were peaks in the spectrum around 15 and 70 meV for which they had no explanation. These peaks were probably caused by the introduction of impurities into the barrier as a result of dirty fabrication techniques.

5. Conclusions

We have shown that inelastic electron tunnelling may be used to obtain information on the vibrational and structural properties of amorphous germanium. The matrix element for coupling the vibrational states to the tunnelling electrons has been calculated, using a bond model for the vibrational modes. This model includes nearest-neighbour correlations and assumes that the disorder in the material is sufficient for the scattering of the electrons from different bonds to be uncorrelated. The calculated matrix element allows the determination of the density of vibrational states from the experimental measurements. The results suggest that the amorphous germanium in the tunnel junctions has an unusually broad distribution of bond angle variations.

It should be noted that the calculation for amorphous germanium may be directly applied to amorphous silicon.

This work establishes inelastic tunnelling spectroscopy as a valuable technique for the study of the amorphous state.

Acknowledgments

This work is supported by SERC through studentships for A F J Levi and M C Payne and a research grant.

References

Adler J G and Straus J 1975 *Rev. Sci. Instrum.* **46** 153
Alben R and Weaire D 1972 *Phys. Rev. Lett.* **29** 1505
Alben R, Weaire D, Smith J E Jr and Brodsky M H 1975 *Phys. Rev.* B **11** 2271
Burt M G and Inkson J C 1976 *J. Phys. D: Appl. Phys.* **9** 43
Cochran W 1965 *Phonons in Perfect Lattices and Lattices with Point Imperfections* ed. R W H Stevenson (Edinburgh: Taylor and Francis)
Etherington G, Wright A C, Wenzel J T, Dore J C, Clarke J H and Sinclair R N 1982 *J. Non-Cryst. Solids* **48** 265
Harrison W A 1966 *Pseudopotentials in the Theory of Metals* (New York: Benjamin)
Heine V and Jones R O 1969 *J. Phys. C: Solid State Phys.* **2** 719
Inkson J C 1980 *J. Phys. C: Solid State Phys.* **13** 369
Jaklevic R C and Lambe J 1966 *Phys. Rev. Lett.* **17** 1139
Kelly M J 1980 *Solid State Physics* vol 35 295
Klein J, Leger A, Defourneau D and Sangster M J L 1973 *Phys. Rev.* B **7** 2236
Ladan F R and Zylbersztejn A 1972 *Phys. Rev. Lett.* **28** 1198
Levi A F J, Phillips W A and Adkins C J 1983 *Solid State Commun.* **45** 43
Meek P E 1977 *PhD Thesis* Cambridge University
Mook H A 1983 private communication
Payne M C and Inkson J C 1983 *J. Phys. C: Solid State Phys.* **16** 4259
Spicer W E 1974 *Amorphous and Liquid Semiconductors* ed. J Stuke and Brenig W (London: Taylor and Francis) p 499
Walmsley D G 1980 *Vibrational Spectroscopy of Absorbates: Springer Series in Chemical Physics* vol 15, ed. R F Willis (Berlin: Springer)
Weaire D and Taylor P C 1980 *Dynamical Properties of Solids* vol 4 ed. G K Horton and A A Maradudin (Amsterdam: North Holland)
Weinberg W H 1982 *Vibrational Spectra and Structure* vol 11 ed. J R Durig (Amsterdam: Elsevier)
Wolfram T 1978 *Inelastic Electron Tunnelling Spectroscopy: Springer Series in Solid State Sciences* vol 4 (Berlin: Springer)